Hindawi
Shock and Vibration
Volume 2023, Article ID 6335011, 14 pages
https://doi.org/10.1155/2023/6335011

Research Article

Evaluating the Effectiveness of a New Self-Centering Damper on a Knee Braced Frame

Seyed Mohammad Banihashem, Moein Rezapour, Reza Attarnejad, and Mahsa Sanei

School of Civil Engineering, University of Tehran, Tehran, Iran

Correspondence should be addressed to Seyed Mohammad Banihashem; seyed.banihashem@ut.ac.ir

Received 2 December 2022; Revised 13 February 2023; Accepted 18 February 2023; Published 29 March 2023

Academic Editor: Cheng Fang

The use of shape memory alloys (SMAs) has been receiving increasing attention among researchers due to their special properties. One of the most important features of SMA is the superelastic behavior which causes the alloy to be able to remove all the applied deformation. This study is intended to evaluate the application of superelastic Nitinol in knee braced steel frames (KBF) as a damper. To fulfill the objective of this research, an experimental KBF system has been developed in ABAQUS using the microscopic finite-element method (FEM). The proposed superelastic damper is placed between the knee element and beam-column connection. Five SMA dampers with different stiffness are located in the KBF system and subjected to static cyclic loading. The hysteresis diagram obtained from this cyclic loading indicates that the damper increases the system strength. The greater the stiffness of the SMA damper, the higher the strength is. Furthermore, the superelastic alloy reduces the permanent deformation and the dissipation energy capacity of the KBF system. Totally, the SMA-equipped KBF system indicates a little lower energy dissipation capacity compared to the KBF system. However, based on the hysteresis diagrams, the reduction of residual deformation in all models is significant compared to the little reduction in energy dissipation. Therefore, the proposed SMA damper is capable of reducing the permanent deformation of the KBF system and maintaining the energy dissipation capacity at almost the same level, which is essential for keeping the structure stable.

1. Introduction

Lateral loads such as earthquake-induced forces play a major role in the design of structures, especially in countries located in the seismic region. To ensure the structural stability and decrease the possible damages, there should be a system that could safely dissipate a significant part of the energy imposed on the structure by plastification process and/or energy dissipation. One of the most well-known strategies that can absorb a significant part of the earthquake force is using steel braces which increase the structural stiffness. To increase energy dissipation capacity, dampers can be utilized within the braces. Most recently, a new damping system called knee braced frame (KBF) has been developed to eliminate the defects of other bracing systems and improve seismic behavior. The knee bracing system mainly needs displacement to dissipate energy through the plastification process. Despite many advantages that this kind of dampers has, they experience lots of damages after an earthquake and need to be replaced. Hence, it is so important to propose a solution to improve the behavior of the knee braced system by using some ductile materials.

In recent decades, researchers have been conducting extensive research works on the feasibility of using a new form of intelligent material called shape memory alloys (SMAs) in structural engineering. Due to these materials' particular behaviors, their application in industry is expanding. SMAs can withstand corrosion, fatigue, and large deformations.

SMAs have got two important properties, shape memory effect and superelastic behavior. The most important characteristic that distinguishes SMAs from other materials is their ability to recover permanent deformation after unloading by heating and returning to the original shape,

which is called shape memory effects and can be classified as a smart control system [1].

In the superelastic behavior which is considered in this study, SMA does not require heating to remove the residual strain. Boroschek et al. utilized Cu-based SMA wires in a three-story steel frame as diagonal braces and studied its seismic behavior on a shaking table. According to their study, SMA in the superelastic mode can enhance the seismic performance of the structure and decrease permanent deformations [2]. Lafortune et al. compared the effectiveness of conventional steel and SMA braces using small-scale experimental tests [3]. They also explored the SMA brace prestraining effects on the structural response. Dolce et al. used this material in a base isolation system and evaluated the structural performance of different isolators [4, 5]. Choi et al. used this new isolation system in the bridges [6] to protect them from the damages caused by earthquake. Their analytical studies on a steel bridge illustrated that the combination of an SMA and a rubber bearing can effectively decrease the dynamic response of a bridge. Ghassemieh et al. evaluated the effectiveness of SMA on coupled concrete shear walls. Their studies indicated that SMA could reduce the damage to the concrete in the walls [7–9]. They also examined these alloys in posting a masonry wall and the results showed that the strength of the masonry wall improved [10]. Hesami and Sadeghi presented a finite-element analysis in which the SMAs were used as dowel bars on the jointed concrete pavements and used fatigue resistance property of SMA [11]. Asgarian and Moradi investigated the seismic performance of steel frames equipped with superelastic SMA braces [12–14]. Johnson et al. studied the application of SMA bars instead of steel bars in the plastic hinge. They examined the superelastic performance of Nitinol, as reinforcement in concrete beams, and showed Nitinol has got this ability to recover and reduce permanent deformations [15–17]. Mortazavi studied the effect of this material on the overall behavior of slit and knee damper [18, 19]. Fang et al. used Nitinol bolts for self-centering connections against seismic action, with the main focus on the influence of composite slab systems on the connection performance [20, 21]. Mishra et al. improved the performance of tuned mass damper (TMD) by using nonlinear superelastic SMA in dissipating energy through a hysteretic phase [22]. Ozbulut et al. used the shape memory alloy (SMA) bracing system to minimize the seismic response of a three-story steel frame [23]. It was shown that SMA provides a suitable recentering mechanism for the structure to return to its original position after a seismic event. Qiu et al. evaluated the seismic performance of knee braced frames equipped with steel or NiTi buckling-restrained braces. The major advantage of NiTi BRBs over steel BRBs is that they successfully eliminated residual drift ratios for the protected frames, which means the KBFs with NiTi BRBs have higher seismic resilience [24].

The knee bracing is a relatively new system in which the diagonal brace is anchored to a short member instead of beam-column joint. This system has been investigated as a new seismic-resistant structural system by several researchers. Conti et al. proposed a plastic design method for seismic resistant knee braced frames [25]. Hsu et al. experimentally utilized cyclic loading to evaluate the performance of steel knee braced frame structures [26]. Furthermore, Mofid and Khosravi conducted several research works on the nonlinear behavior of KBF system and presented an approximate method to predict that behavior [27–29]. In another study, Amer et al. used KBF to retrofit a four-story reinforced concrete building and improve the seismic performance [30]. Aniello and Landolfo studied the influence of using different knee bracing systems, e.g., chevron and diagonal braces to improve the structural response of an existing steel frame through nonlinear time history analysis [31].

The objective of this study is to evaluate the effects of superelastic Nitinol damper on the seismic behavior of a KBF system; ABAQUS finite element software is used for modeling and analysis of the proposed system. SMAs have an effect on the resistance and permanent deformation based on their length, and these two parameters have a great effect on the capacity of energy dissipation. The main focus of this article is to investigate the direct and inverse effects of SMA damper on energy dissipation capacity.

2. Shape Memory Alloy (SMA)

SMA's atomic structure causes a unique behavior that distinguishes this alloy from other materials. SMAs have two different atomic phases, namely, austenite and martensite. Austenite is stable at high temperatures and low stress, and martensite is stable at low temperatures and high stress. SMAs have two important characteristics: the shape memory effect (SME) and the superelasticity (SE) [32]. In the superelastic behavior, the aforementioned phases can reversibly switch to each other during cyclic loading (Figure 1). Many types of SMAs have been introduced so far, but nickel-titanium is the most suitable one for seismic applications due to its remarkably superelastic effects (In this article, SMAs are mostly referred to as Nitinol).

Some parameters should be used to define the superelastic effect in ABAQUS. Modulus of elasticity of SMA in the austenite and martensite phases (E_A, E_M) and Poisson's ratios (ν_A, ν_M) simulate the linear behavior of SMA. The nonlinear part is defined by transformation stresses (σ_{Ms}, σ_{Mf}, σ_{As}, and σ_{Af}), and the maximum transformation strain ε_L. The four stresses values at a constant temperature are as follows: austenite to martensite starting stress (σ_{Ms}), austenite to martensite finishing stress (σ_{Mf}), martensite to austenite starting stress (σ_{As}), and martensite to austenite finishing stress (σ_{Af}). The schematic stress-strain diagram for the superelastic behavior is shown in Figure 1. When the temperature is high enough, the atomic structure at the beginning of the loading path is austenite. During loading, when the stress reaches the limit of σ_{Ms}, the atomic structure starts changing from austenite to martensite. At this stage, the alloy strength decreases until it reaches σ_{Mf}, and the structure completely shifts to the martensite phase. The alloy stiffness in this region is equal to E_M. In the unloading path, when the stress reaches σ_{As}, the atomic structure changes from martensite to austenite, and at this stage, the

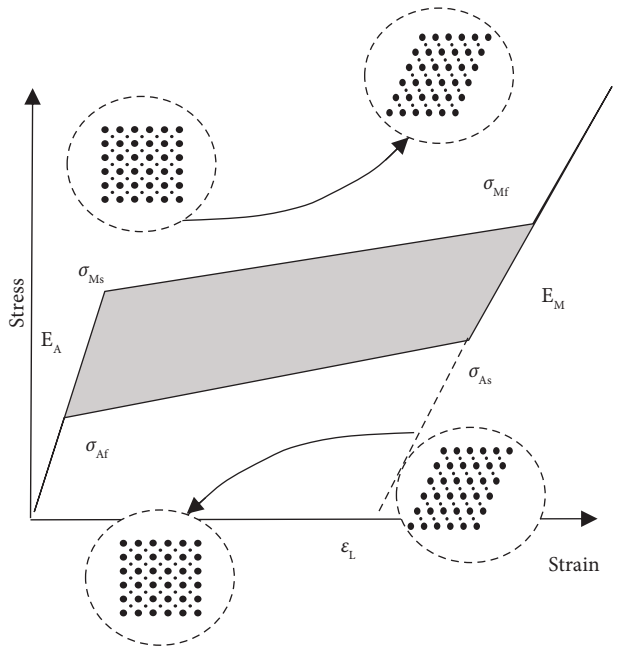

Figure 1: Stress-strain diagram of a typical superelastic SMA [9].

permanent deformation is eliminated entirely showing that when the stress reaches σ_{As}, the stiffness equals E_A and SMA returns to its original shape [33].

3. Knee Braced Frame (KBF)

One of the most practical hysteretic dampers is the knee damper that dissipates the imposed energy by yielding in the oblique knee element attached to the brace. In this damping system, the major portion of nonlinear behavior occurs in the knee and this part experiences most of the damage while the brace remains almost linear. It should be noted that the dimension properties of the knee such as size, diameter, length, and even angles directly affect the frame behavior and the system damping capacity.

Energy dissipation in this system is mainly in the form of moment plastic hinge. The areas where nonlinear behavior occurs are mainly at the two ends of the knee and its connection to the brace. The dimensions selected for the knee brace should be such that the brace does not buckle during the loading. Therefore, a limit should be considered for the dimensions of the knee so that all nonlinear shape changes occur in the knee damper. One of the advantages of this system is that after the end of the lateral loading, the major damage occurred in the knee and the rest of the system components remain almost intact. Therefore, by replacing it, the system can be easily restored. It is also very easy to access for replacement.

4. KBF Model

To investigate the effects of SMA on the KBF damper, a large-scale model of a KBF system which is experimentally tested by Balendra et al. is selected [34]. Figure 2 illustrates the geometry of this experimental study.

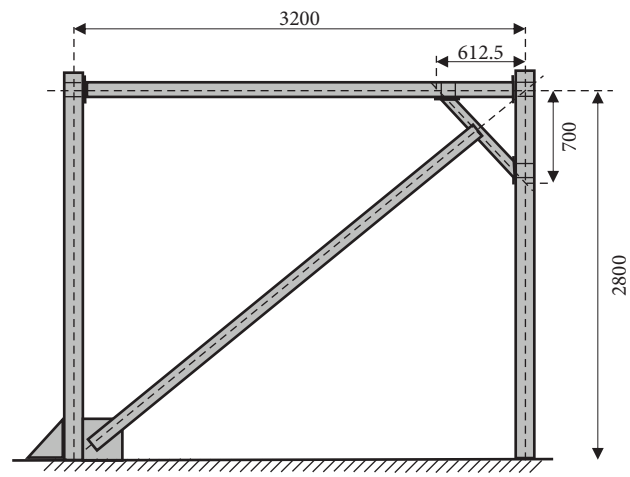

Figure 2: The KBF system made by Balendra (dimensions in mm).

The column and beam sections were selected in such a way that they remain elastic during loading. Wide flange sections WF $100 \times 100 \times 17.2$ kg/m and WF $125 \times 125 \times 23.8$ kg/m were selected for the columns and the beam, respectively. A 20 mm thick plate was inserted at the beam-column connection as a stiffener. To prevent web buckling, transverse stiffeners were welded to the column at the beam-column joint. The brace must resist compression without buckling and remain elastic in tension. Hence, the brace used in the frame is made of two C-channels $100 \times 50 \times 5$ mm, laced together by $12 \times 38 \times 10$ mm plates at the longitudinal spacing of 200 mm. Since the dissipated energy is provided by yielding in the knee element, the structural design of this part is of special importance. The only way to make this yielding procedure possible is to provide sufficient rotational capacity. Therefore, a square hollow section SHS $60 \times 60 \times 4.5$ mm was chosen for the KBF damper by Balendra. It was found that this section would satisfy the lateral-torsional buckling criterion. Balendra also put a 15 mm thick plate at the knee-beam and knee-column joint to facilitate the replacement of the knee. Also, at the knee-beam and knee-column connections, as can be seen in Figure 2, web stiffeners were welded to the beam and column to protect them from local buckling [34].

All elements of the structure, except for the knee, are made of steel with a yield stress of 350 MPa. The steel used in the knee damper has a yield stress of 417 MPa. The modulus of elasticity and Poisson's ratio of the steel are 190 GPa and 0.3, respectively.

In the Balendra study, a sinusoidal base excitation load was applied on the frame to simulate earthquake-induced forces. The excitation frequency was 20 rad/s. The initial amplitude of the excitation was 2.25 m/s^2, and this amount was increased by 0.79 m/s^2 after every five cycles. The displacement-time history of the applied loading is shown in Figure 3.

5. Numerical Modeling

Since ABAQUS is able to solve nonlinear problems under static, dynamic, and quasi-dynamic loading considering large deformations, this software is used to simulate the proposed KBF system. In the FEM modeling, two types of

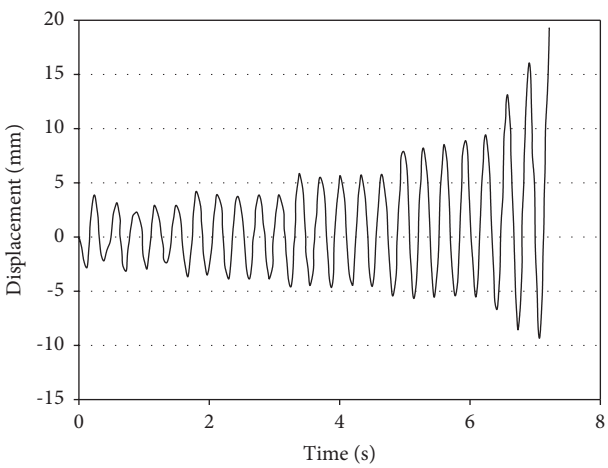

Figure 3: Inelastic displacement-time history [34].

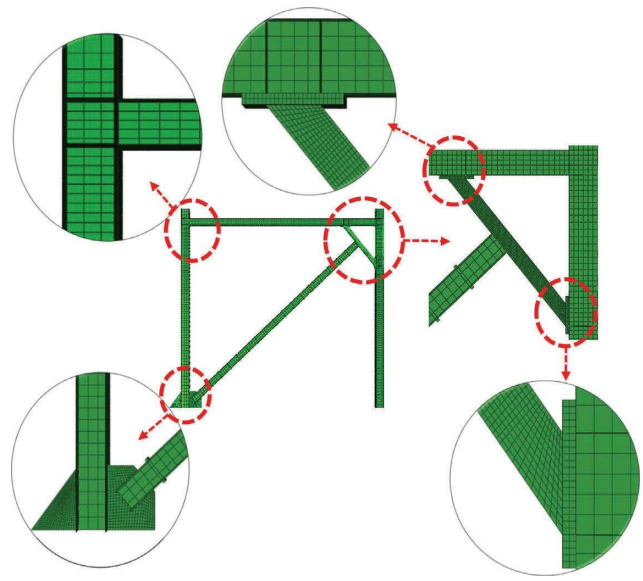

Figure 4: FEM modeling of the KBF system in ABAQUS.

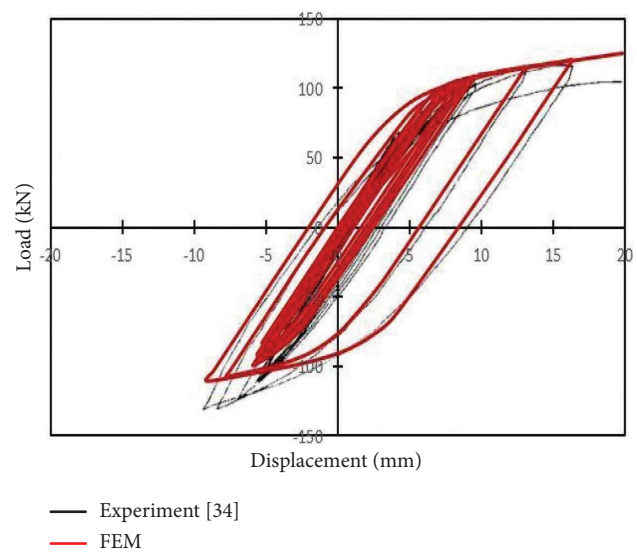

Figure 5: Load versus displacement of the experimental study and FEM model [34].

eight-node solid (C3D8) and four-node shell (S4R) elements are used. The solid elements are used to simulate the knee damper since this part requires a more accurate calculation and the shell elements are utilized in other parts of the frame. Reduced integration is assigned to the shell elements to decrease the runtime of the analysis. One of the most important keys in modeling is to specify how the elements interact with each other. Therefore, all parts of the frame, except for the knee, should be merged. The knee contact surfaces with the beam, column, and diagonal brace are defined by tie interaction, in which the relative displacements of the knee elements are bound in three directions.

Meshing is an integral part of the simulation process. It influences the accuracy, convergence, and speed of the analysis. In this study, the mesh size is considered to be about 5 cm in places away from the joints where plastic deformation is not anticipated. By approaching the damper connections, the mesh size is reduced to 2 cm. Since the plastic behavior in the knee element is more important than other places, the mesh size in this part ranges from 6 mm to 10 mm. To define the boundary conditions, the base of the columns is assumed to be fixed in three directions, and the horizontal load is applied to the beam center line (Figure 4).

Figure 5 illustrates the comparison of load versus displacement obtained from the finite-element analysis and experimental study. According to this figure, the finite-element model has been able to accurately predict the nonlinear behavior of the frame.

To evaluate the effect of the superelastic damper on the KBF system in this study, a Nitinol SMA which was tested by DesRoches et al. is selected [35]. The atomic structure of the Nitinol was austenite at the room temperature, so the Nitinol behavior was superelastic. The mechanical properties of Nitinol are presented in Table 1. Nitinol is used as a self-centering damper in this study and the same geometric and mechanical properties of the SMA are modeled in the ABAQUS by a truss element. The cyclic loading presented in Figure 6 is applied to both a Nitinol wire and the experimental SMA. The result of this loading is illustrated in Figure 7. According to which, the FEM model simulates the experimental SMA behavior with an acceptable accuracy.

In this study, a two-way cylindrical SMA damper is proposed. Figure 8 shows the internal parts of the damper. The recommended damper is made of steel. These elements are almost rigid and show little deformation against SMA wires. Figure 9 illustrates the shape and dimension of the five main parts of the suggested damper.

The recommended damper is designed to be always in tension since the SMA wires buckle under compression. Qiu and Zhu proposed a similar damper in which SMA wires are under tension during the loading [36]. According to Figure 10, the disk-shaped segments (Numbers 1 and 2) are located at the ends of the cylinder and the SMA wires are attached to them. There are two bulges inside the cylinder to

Table 1: Mechanical properties of the superelastic SMA [35].

Diameter (mm)	Length (mm)	A_s (°C)	E_A (GPa)	σ_{Ms} (MPa)	σ_{Mf} (MPa)	σ_{As} (MPa)	σ_{Af} (MPa)
1.8	152	−26	40	538	573	104	69

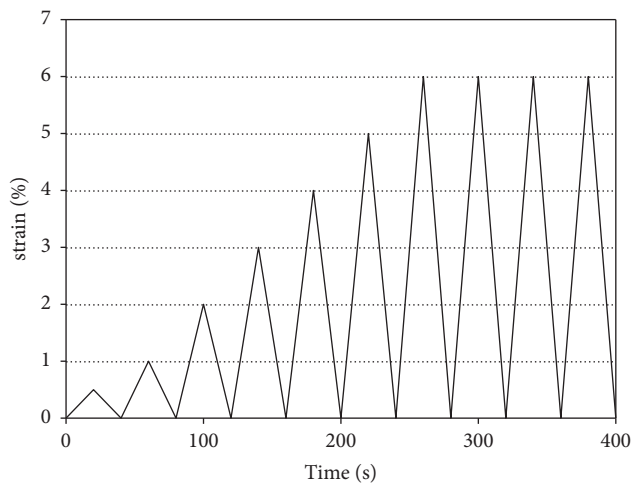

Figure 6: Cyclic loading applied to the SMA.

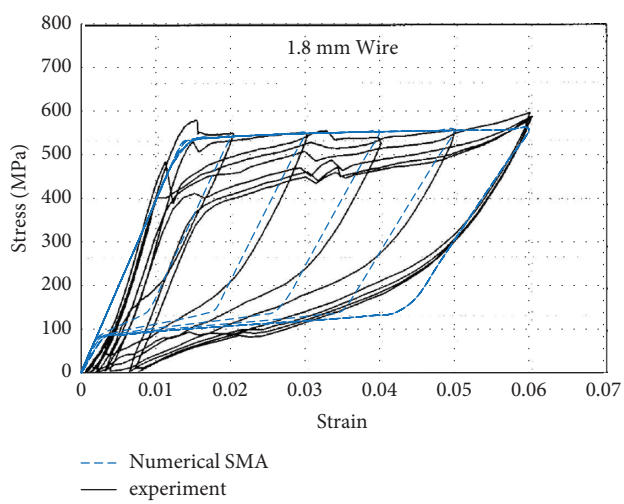

Figure 7: The SMA superelastic behavior.

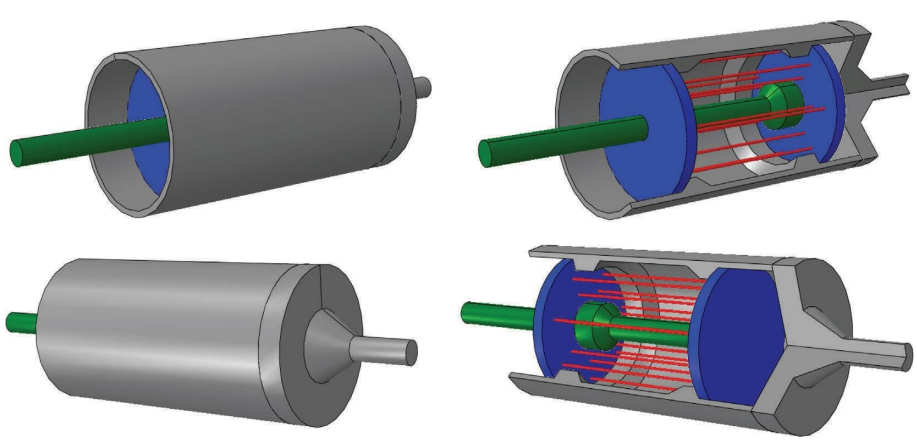

Figure 8: The recommended damper equipped with SMA wires.

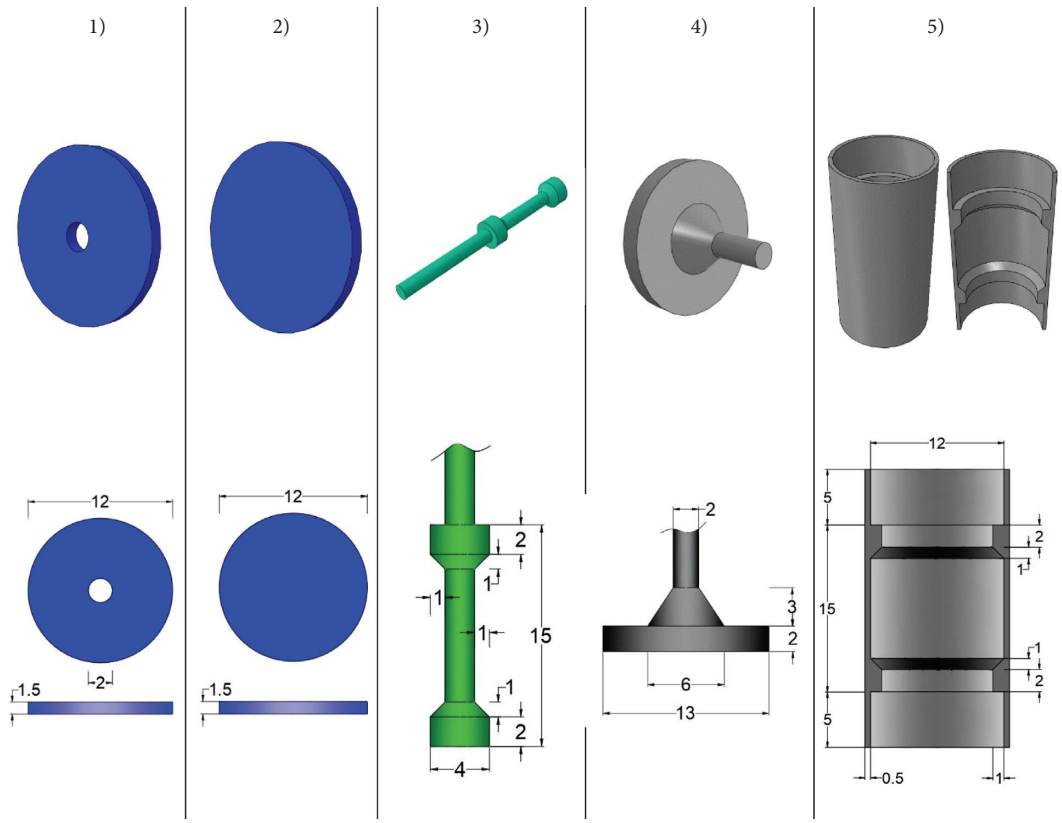

Figure 9: The elements of intelligent recommended damper (dimensions in cm).

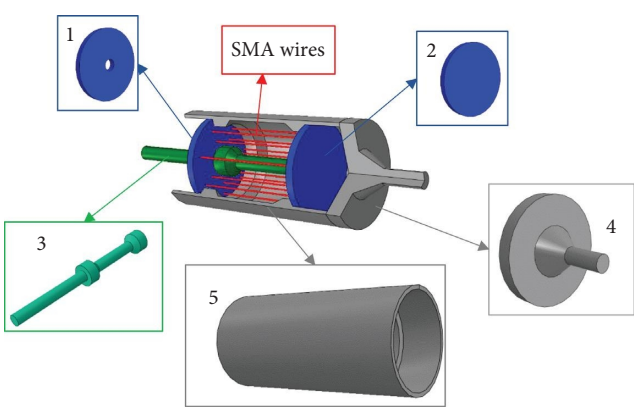

Figure 10: Assembling of the suggested damper.

restrict the movement of elements number 1 and 2. A bar (Number 3) passes through segment number 1 and its end is located next to segment number 2. Segment numbers 4 and 5 make the damper's body.

According to Figure 11, when the damper is compressed, segment number 2 moves forward and segment number 1 remains fixed. Reversibly, while the damper is under tension, segment number 1 moves backward and segment number 2 remains in its position. In both cases, the assembling of SMA wires is in such a way that they always be in tension as it has been mentioned earlier.

Solid and truss elements were used to model the damper in ABAQUS. Solid elements were used in the cover, middle bearing rod and two ends of the circular damper. The truss element was also used to model the SMA wires. The interaction between the plates was considered as surface to surface and its mechanical characteristics are frictionless and hard contact.

To reduce the time of analysis in ABAQUS software, the truss element which simulates the microscopic behavior of SMA damper is used instead of exact modeling (Figure 12). Because of the installation of the damper in Figure 8 in the numerical model greatly increases the degree of freedom of the model. In order to simplify, the proposed damping behavior was applied to the structure as a truss element. As the degree of freedom decreases, the stiffness matrix of the structure shrinks, which reduces the time for model analysis [37, 38].

In this study, six models, KBF1, KBF2 up to KBF6, have been developed to investigate the effect of SMA on the knee damper behavior. KBF1 is the model that was verified by Balendra experimental work and does not contain any superelastic damper. In other models, as seen in Figure 13, the superelastic damper is attached to the knee dampers. At this place, the deformation between the knee and beam-column joint is greater with respect to other locations. Since the SMA damper requires a great amount of deformation to dissipate energy, the damper is placed here.

The main differences between SMA-equipped damper models are in the amount of SMA and the knee geometric properties. The dimensions of these elements have been

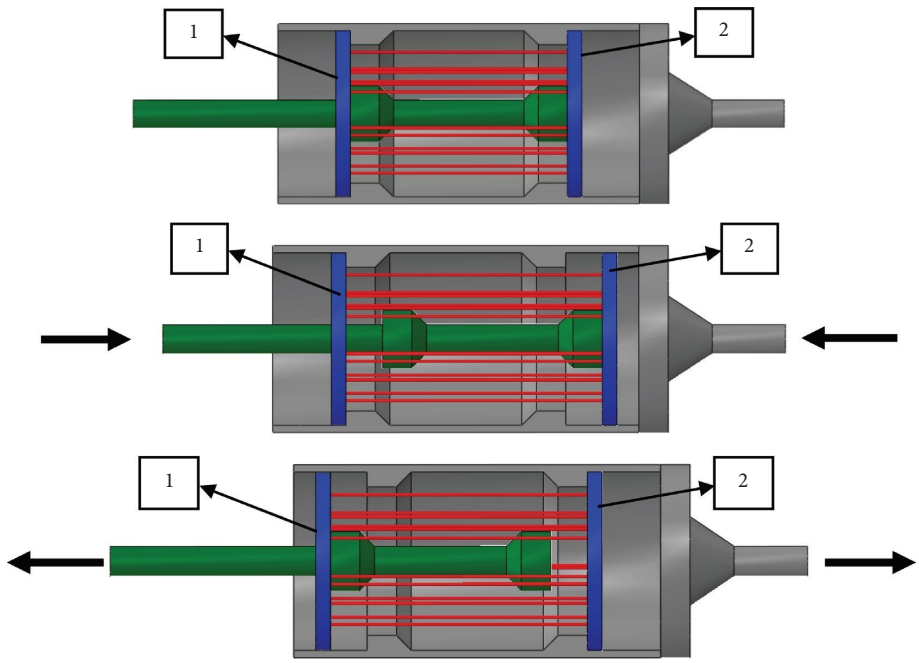

Figure 11: The performance of the suggested damper under tension and compression.

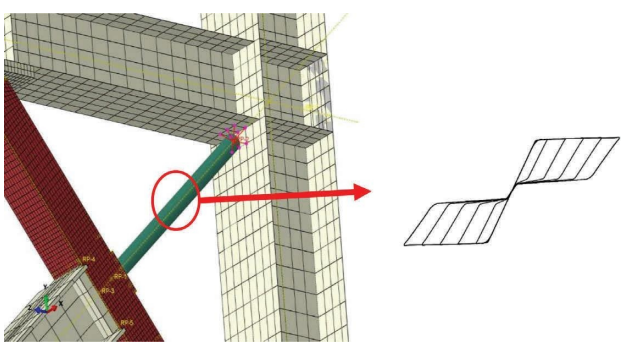

Figure 12: Placing the SMA damper between knee and beam-column connection.

chosen in a way that with the increase in SMA damper stiffness, the knee stiffness decreases the same amount. The reduction of the knee element's stiffness is assigned to the model by reducing the knee dimension. Table 2 shows the knee dimensional and mechanical properties of the knee element and Nitinol wires in the SMA damper.

To calculate the stiffness of the proposed system, the knee and SMA dampers are considered parallel to each other (Figure 14). In Figure 14, E_k and E_s are the modulus of elasticity of steel and SMA, I and A are the knee moment of inertia and the Nitinol area, respectively, and L is the length of the SMA damper. According to this figure, blue parts of the SMA damper are rigid and have higher stiffness compared to SMA. The knee and SMA stiffness (K_{knee} and K_{SMA}) are calculated from the following equations and based on that, the SMA area and the knee section geometry are selected in such a way that the sum of the SMA and knee stiffness remain constant (Table 2).

$$K_{knee} = \frac{3E_k I\,(a+b)^3}{a^3 b^3},$$
$$K_{SMA} = \frac{E_s A}{L}. \tag{1}$$

6. Numerical Results

Since the load applied to the experimental model was quasi-dynamic and the nonlinear deformation was not significant, the models were subjected to the nonlinear static cyclic loading based on the ATC-24 protocol (Figure 15). It is one of the first formal protocols which were developed in the U.S. for seismic performance evaluation of steel structural elements under cyclic loading [39]. According to Figure 15, this protocol consists of seven displacements, the first five drifts, are repeated three times each, and the last two drifts, are repeated twice. The deformation proposed in this protocol is greater with respect to the quasi-dynamic loading. Since the maximum displacement of the frame due to this loading is about 3 cm which is approximately two times greater than the displacement from experimental quasi-dynamic loading; in large cycles, the damage occurs with fewer repetitions [40].

In Figure 16, the cyclic behavior of KBF1 under ATC-24 loading is presented. According to this figure, the dissipated energy has increased dramatically due to the significant increase in displacement compared to the experimental quasi-dynamic loading. Figure 16 also shows the cyclic behavior of KBF2 to KBF6 SMA-damper equipped models. It indicates that the SMA dampers have been able to reduce the permanent deformation and turn the hysteresis curve into a flag shape. There is some asymmetricity in the last cycle of hysteresis in KBF6 that occurs due to the knee top

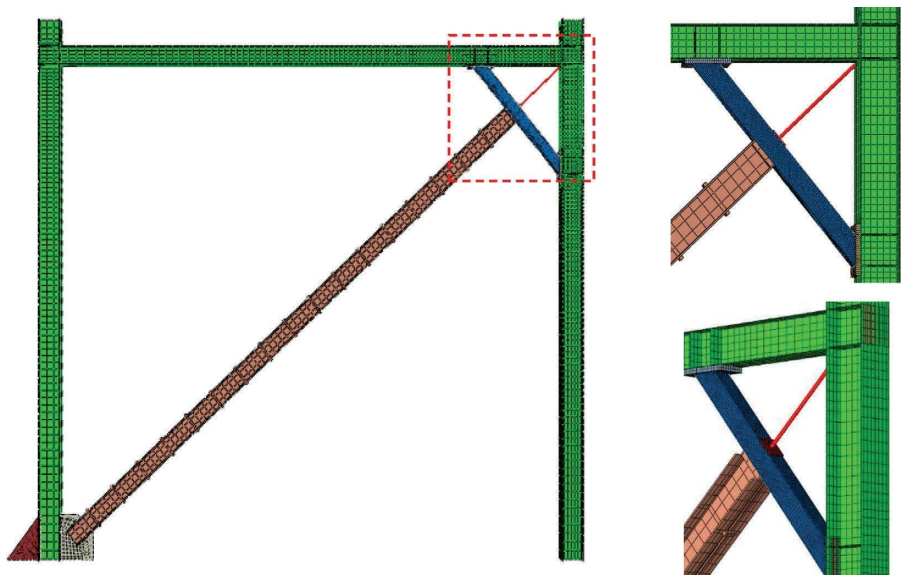

Figure 13: General configuration of KBF2 to KBF6.

Table 2: Dimensional and mechanical properties of the knee element and SMA wires.

	Knee dimensions (mm)	Knee stiffness (N/mm)	SMA (mm)	SMA stiffness (N/mm)	Knee stiffness + SMA stiffness (N/mm)
KBF1	60 ∗ 60 ∗ 4.5	64850			64850
KBF2	55 ∗ 55 ∗ 4	44401	30 D1.8	20347	64748
KBF3	55 ∗ 55 ∗ 3.5	38851	39 D1.8	26451	65302
KBF4	52 ∗ 52 ∗ 3.5	32834	48 D1.8	32556	65390
KBF5	50 ∗ 50 ∗ 3	25019	59 D1.8	40016	65036
KBF6	50 ∗ 50 ∗ 2.5	20850	65 D1.8	44086	64935

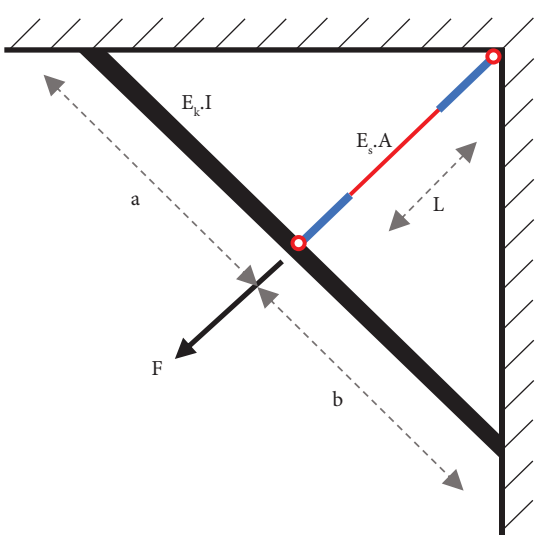

Figure 14: Considering the knee and SMA damper as parallel springs.

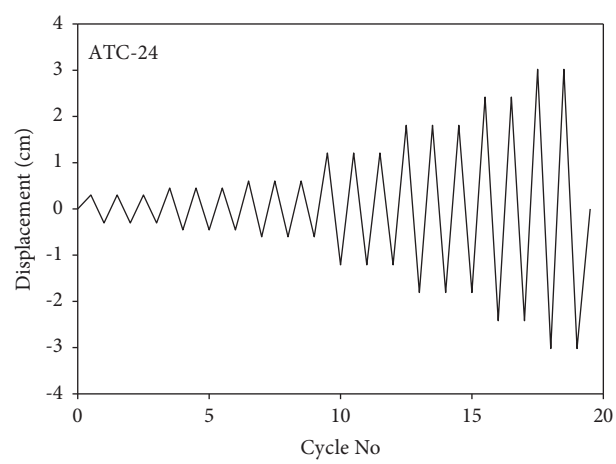

Figure 15: The system-applied loading protocol.

plate yielding (Figure 17). In this model, the SMA damper stiffness is about 2.1 times greater than the knee damper stiffness which causes the knee to absorb more plastic deformation. The plastic deformation can be postponed by placing more stiffeners within the knee plastic area. However, using stiffeners is ignored in KBF6 to make the condition of the models similar.

Regarding the results presented in the cyclic behavior curves under ATC-24 loading, the permanent deformations have reduced significantly. This reduction results in less energy dissipation capacity; on the other hand, the SMA damper has increased the system resistance, which can improve the energy dissipation capacity of the system.

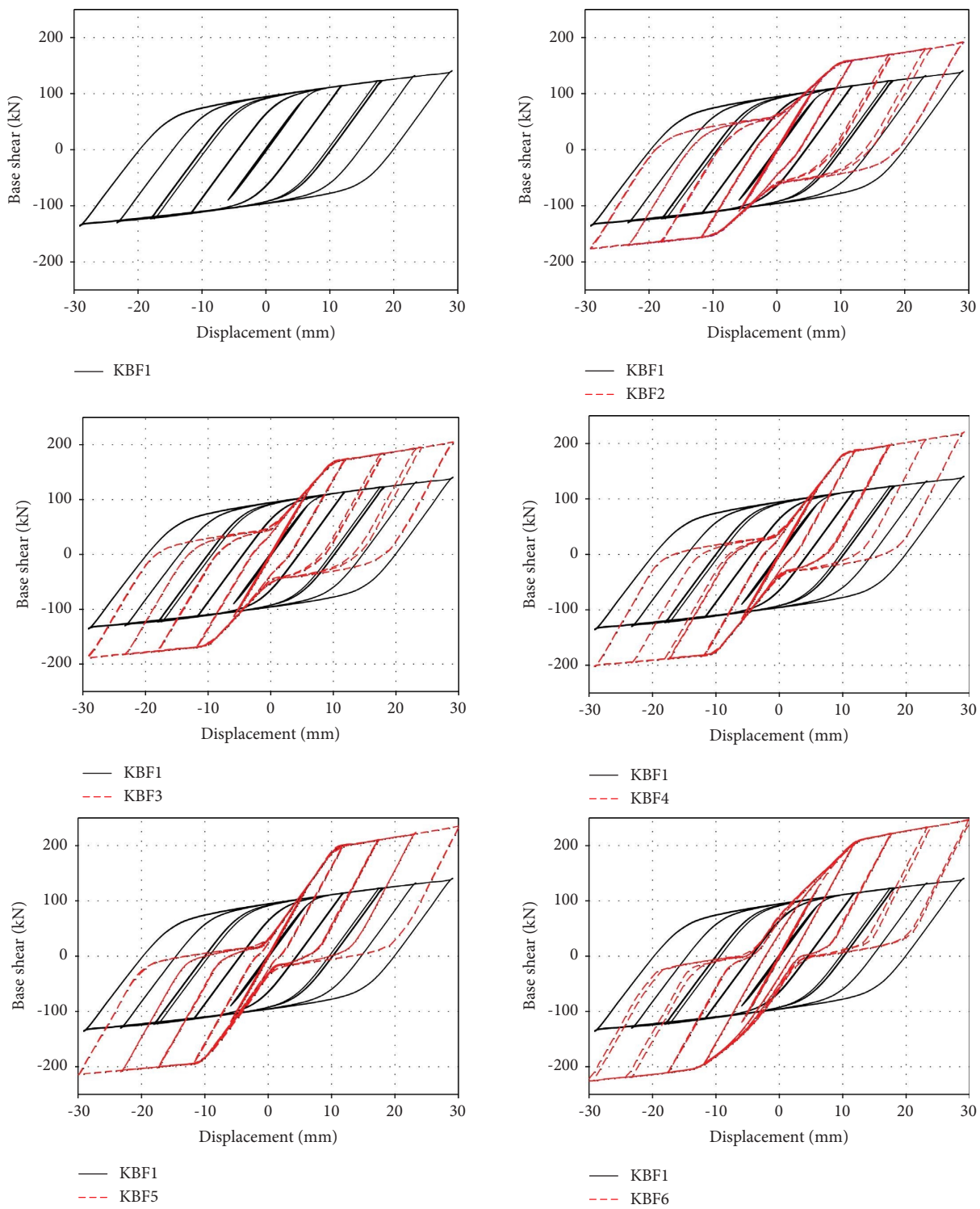

Figure 16: Hysteresis diagrams of the numerical models.

As previously mentioned, the cross-sectional area of SMA and knee are selected in such a manner that the stiffness of all models is almost equal. On the other hand, the SMA yield strain is higher than that of steel. The model stiffness together with SMA yield strain (which is greater than that of steel) causes the yield base shear of the SMA-equipped models to be higher compared to KBF1. Figure 18 presents the yield strength and the corresponding displacement for all models and illustrates that the greater the cross-sectional area of SMA wires, the greater the yield displacement is.

The studied system under lateral load has two yielding displacements. In the first (Δ_{y1}), one of the two dampers experiences nonlinear behavior, and in the second (Δ_{y2}),

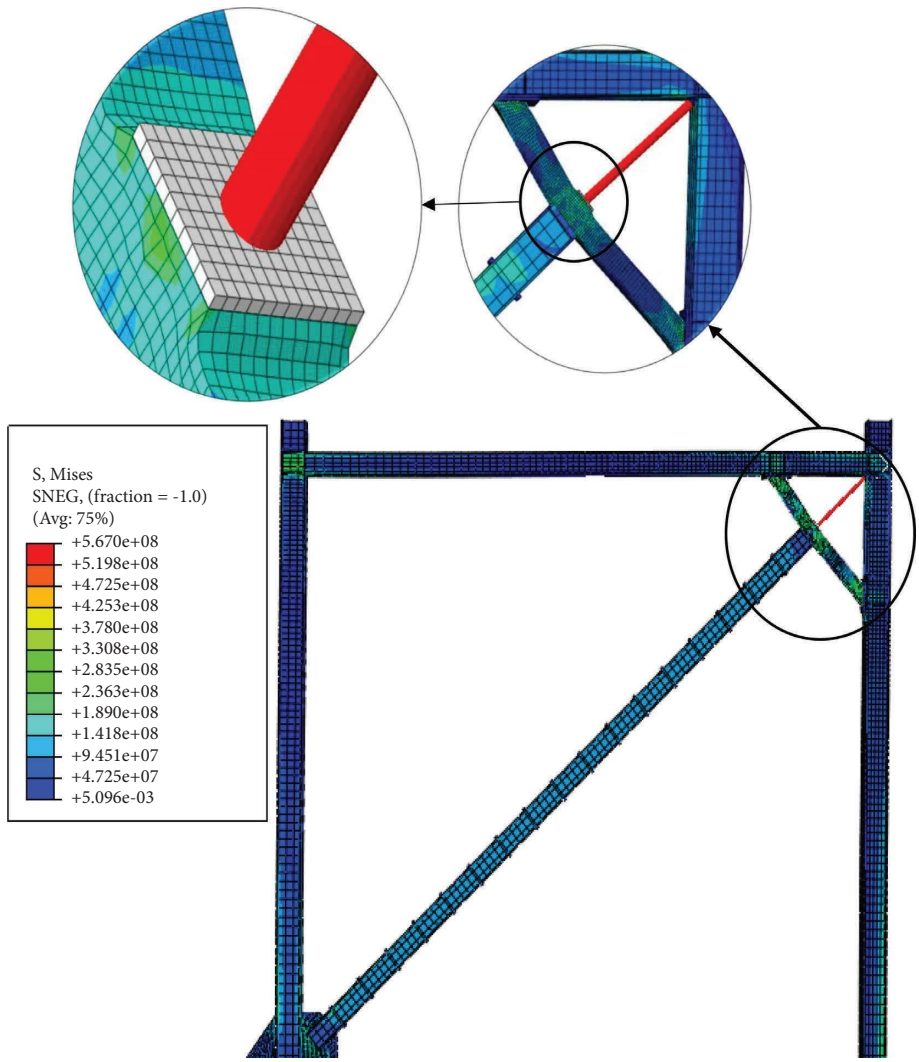

Figure 17: The yielding of top plate in KBF6.

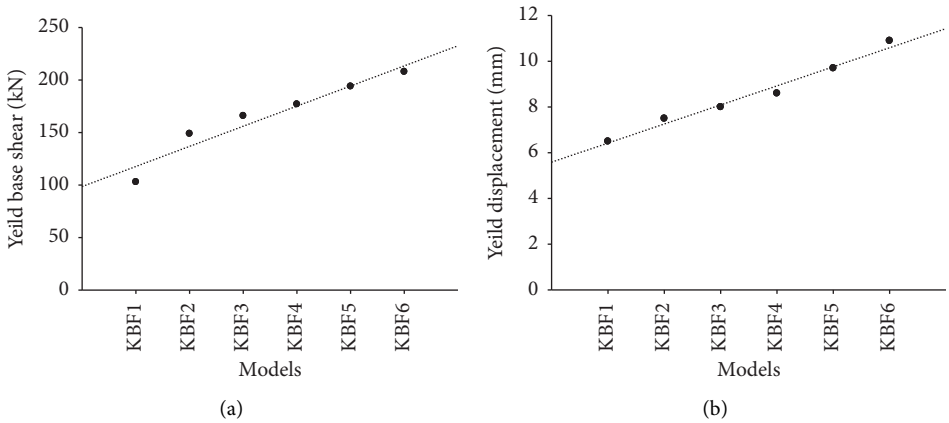

Figure 18: (a) The model's yield base shear. (b) The model's yield displacement.

Table 3: The amount of dissipated energy in cyclic loading (kN).

Cycle nos.	KBF1	KBF2	KBF3	KBF4	KBF5	KBF6
1	0.27	0.17	0.17	0.16	0.15	0.16
2	0.32	0.19	0.19	0.18	0.16	0.17
3	0.35	0.23	0.22	0.21	0.20	0.21
4	3.79	2.78	2.61	2.52	2.56	3.65
5	4.60	3.45	3.24	3.13	3.18	4.54
6	4.65	3.51	3.30	3.19	3.24	4.61
7	43.52	41.62	37.66	35.76	35.38	39.02
8	53.35	51.55	46.65	44.35	43.82	47.67
9	53.94	52.19	47.28	44.97	44.45	48.33
10	1569.32	1388.27	1248.84	1088.14	918.20	1043.29
11	1779.19	1500.47	1332.10	1147.41	957.53	1208.90
12	1765.22	1482.82	1312.31	1127.35	935.43	1206.87
13	4064.99	3873.97	3702.37	3369.25	3195.71	3483.64
14	4159.65	3962.95	3792.53	3339.40	3162.84	3531.63
15	3963.88	3870.59	3715.66	3483.98	3144.59	3514.37
16	6037.96	6269.20	6101.26	5633.05	5457.13	5961.65
17	6058.89	6028.47	5862.50	5653.90	5476.79	6268.22
18	8188.76	8332.33	8189.58	7971.98	8288.35	8508.91
19	7992.34	8205.57	8086.14	7868.83	8289.44	8360.31
Total	45745.00	45070.33	43484.62	40817.76	39959.13	43236.13

both dampers show nonlinear behavior. It is possible to analytically estimate these displacements of the structure by the following relations:

$$\Delta_{y1} = \frac{\min\left(\sigma_{Ms}L_s/E_s, \sigma_y s.L_k^2/24E_kI\right)}{\cos(\theta)},$$
$$\Delta_{y2} = \frac{\max\left(\sigma_{Ms}L_s/E_s, \sigma_y s.L_k^2/24E_kI\right)}{\cos(\theta)}, \quad (2)$$

where σ_{Ms} and σ_y are the martensite starting stress and steel yielding stress, respectively. L_s and L_k are the length of SMA and knee damper, E_s and E_k are the elastic module of SMA and knee damper, respectively. s is elastic section modulus of knee damper and θ is the angle of the brace with the horizontal axis. The lateral resistance of the system can also be calculated by the following analytical relationship:

$$\frac{F_y}{\cos^2(\theta)} = \left(\left(\frac{E_sL_s}{A_s} + \frac{192E_kI}{L_k^2}\right)\Delta_{y1} + \overline{K}.\left(\Delta_{y2} - \Delta_{y1}\right)\right),$$
$$\text{if}\left(\frac{\sigma_{Ms}L_s}{E_s} > \frac{\sigma_y s.L_k^2}{192E_kI}\right) \longrightarrow \overline{K} = \frac{E_sL_s}{A_s}, \quad (3)$$
$$\text{if}\left(\frac{\sigma_{Ms}L_s}{E_s} \leq \frac{\sigma_y s.L_k^2}{192E_kI}\right) \longrightarrow \overline{K} = \frac{192E_kI}{L_k^3}.$$

The enclosed area in the cyclic curve shows the value of dissipated energy in the structure. For studied models, the amount of energy dissipated in each cycle is shown in Table 3. According to Table 3, in the first nine cycles, the energy dissipation rate is approximately zero. From cycle 10 to 15, the amount of energy dissipation in SMA-equipped models is lower than KBF1, but these numbers increase in the last cycles and in some SMA-equipped models, even become more than KBF1. Therefore, the SMA damper can cause acceptable energy dissipation at large deformations. Usually, in repetitive cycles (with equal displacement), energy dissipation is negligibly reduced due to the loss of structural resistance during cyclic repetition.

According to the last row of Table 3 which shows the total dissipated energy during cyclic loading, as the SMA sectional area increases, the amount of dissipated energy decreases except for KBF6 which is because of the yielding of the knee top plate. Figure 16 illustrates a little asymmetricity in KBF6 that causes an increase in dissipated energy capacity.

Table 3 shows that the KBF systems equipped with SMA dampers have a lower energy dissipation capacity compared to KBF1, but this reduction is not significant, and in larger cycles, the amount of energy absorbed by the system is even close to KBF1.

The most important feature of superelastic SMA is the ability to eliminate permanent deformation imposed on the alloy. The atomic structure of these types of alloys is capable of removing large deformation in cyclic loading both in positive and negative directions. Permanent deformation is important due to the presence of vertical loads (such as dead and live loads) in the structure, which creates additional stresses and structural instability due to the P-delta effect. The superelastic property of the SMA would be effective in the reduction of the lateral displacement and prevention of the additional.

In Figure 16, the permanent deformations of numerical models under cyclic loading are presented. According to Figure 16, by increasing the SMA area, permanent deformation decreases. In most cases, the SMA damper has been able to reduce the residual deformation in comparison with KBF1, although the reduction percentage is not the same in different cycles. Figure 19 shows the reduction percentage of permanent deformations in the SMA-

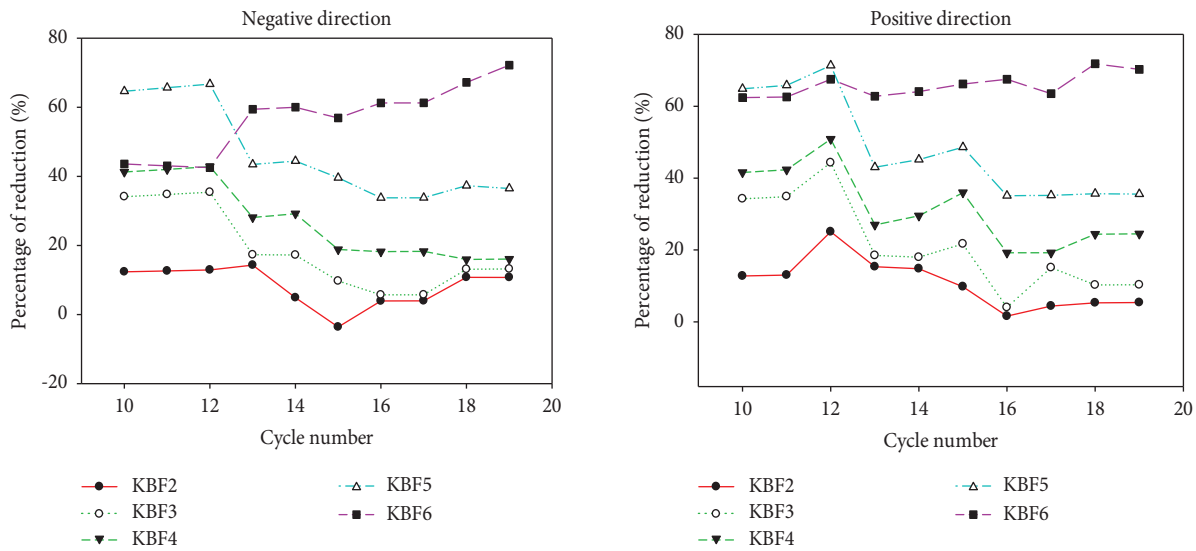

Figure 19: The reduction of permanent deformation in positive and negative directions compared to KBF1.

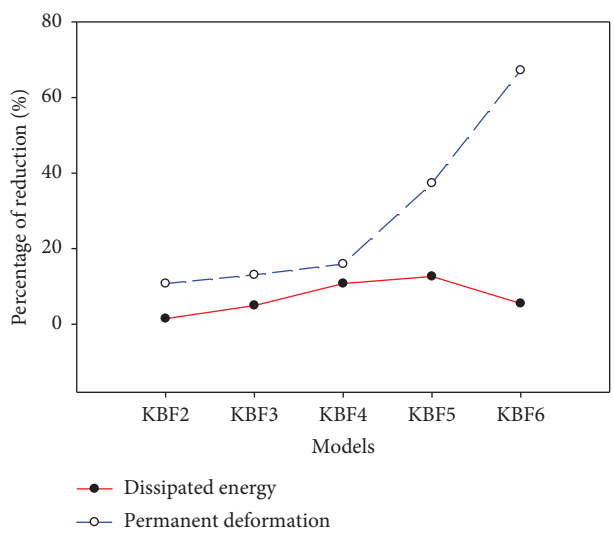

Figure 20: The comparison of reduction in energy dissipation capacity and permanent deformation.

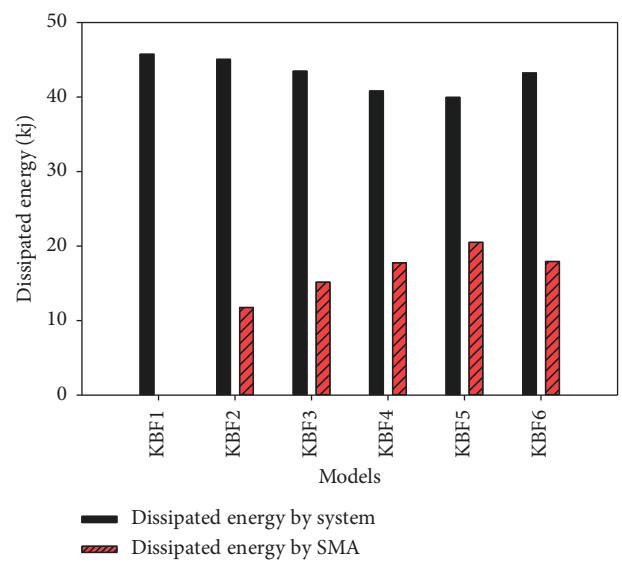

Figure 21: The contribution of the SMA damper in energy dissipation of the proposed KBF system.

equipped model in both positive and negative directions. It indicates that the amount of reduction in the first cycles is higher than the last cycles, except for KBF6 which follows a different pattern.

The energy dissipation capacity of a structure is of great importance and excessive reduction of this value makes the structure vulnerable to earthquakes. According to the presented hysteresis results, the damper in SMA-equipped systems can reduce the amount of residual deformation along with the little reduction in energy dissipation. The SMA damper has been able to increase the system resistance, but it also reduces the permanent deformation. Increasing resistance and reducing permanent deformation, respectively, increase and decrease the energy dissipation capacity. Since the major part of deformation occurs in the last cycle, Figure 20 presents the results of the reduction of the energy dissipation and residual deformation compared to KBF1. According to Figure 20, the amount of energy dissipation has been reduced slightly in the SMA-equipped models, but the permanent deformation has been significantly reduced. In KBF5, the residual deformation and energy dissipation capacity are decreased by 37% and 12%, respectively.

The SMA damper absorbs the main part of the energy applied to the structure, and the knee system absorbs the rest of that. Figure 21 shows the amount of energy absorbed by SMA damper against the total energy entered the structure. Based on Figure 21, as the amount of SMA increases, the energy dissipation portion of SMA increases as well, but in KBF6, since the knee top plate yields very soon, most of the energy is absorbed by the knee element. Therefore, to raise the energy absorption of the SMA damper in KBF6, stiffeners shall be provided.

7. Conclusion

The main purpose of this study is to investigate the effect of smart dampers on knee braced frames. To fulfill this goal, five models with different percentages of SMA damper are considered. Based on the cyclic behavior of the simulated models in this study, the following results have been obtained:

Since the yield strain in Nitinol is greater than that of steel and the stiffness of systems are equal, the yield strength in the smart damper-equipped frame is more than a usual knee braced frame. The increase of SMA stiffness makes the system show higher yield strength.

The increase of SMA contribution in stiffness causes the reduction in residual deformation and energy dissipation capacity which are positive and negative points, respectively. However, in KBF5, for example, the residual deformation decreased by 37% while the energy dissipation capacity had only a 12% reduction compared to KBF1. In fact, the reduction percentage of residual deformation is more than the reduction of energy dissipation capacity in the models with smart damper. Increasing the shape memory alloy contribution by up to 70% results in knee wings failure increases energy dissipation capacity and also reduces the effect of the intelligent damper on the structure. The contribution of intelligent dampers to the total energy dissipation in studied models is between 20% and 50%. On the other hand, with the failure of knee wings, the effect of the shape memory alloys on the overall behavior of the system decreases; this is why in KBF6, the effect of the intelligent damper in energy dissipation is smaller compared to that in KBF5.

Data Availability

The data used in this article are the result of the analysis of numerical models and their validation with the experimental model.

Conflicts of Interest

The authors declare that they have no conflicts of interest.

References

[1] A. R. Shahin, P. H. Meckl, and J. D. Jones, "Modeling of SMA tendons for active control of structures," *Journal of Intelligent Material Systems and Structures*, vol. 8, no. 1, pp. 51–70, 1997.

[2] R. L. Boroschek, G. Farias, O. Moroni, and M. Sarrazin, "Effect of SMA braces in a steel frame building," *Journal of Earthquake Engineering*, vol. 11, no. 3, pp. 326–342, 2007.

[3] P. Lafortune, J. McCormick, R. DesRoches, and P. Terriault, "Testing of superelastic recentering pre-strained braces for seismic resistant design," *Journal of Earthquake Engineering*, vol. 11, no. 3, pp. 383–399, 2007.

[4] M. Dolce, D. Cardone, and F. C. Ponzo, "Shaking-table tests on reinforced concrete frames with different isolation systems," *Earthquake Engineering & Structural Dynamics*, vol. 36, no. 5, pp. 573–596, 2007.

[5] M. Dolce, D. Cardone, F. C. Ponzo, and C. Valente, "Shaking table tests on reinforced concrete frames without and with passive control systems," *Earthquake Engineering & Structural Dynamics*, vol. 34, no. 14, pp. 1687–1717, 2005.

[6] E. Choi, T.-h. Nam, and B.-S. Cho, "A new concept of isolation bearings for highway steel bridges using shape memory alloys," *Canadian Journal of Civil Engineering*, vol. 32, no. 5, pp. 957–967, 2005.

[7] M. Ghassemieh, S. Mohyeddin Ghodratian, M. Reza Bahaari, and S. Ali Nojoumi, "Seismic enhancement of coupled shear walls using shape memory alloys," *Journal of Civil Engineering and Science*, vol. 2, no. 2, pp. 93–101, 2013.

[8] M. Ghassemieh, M. Mostafazadeh, and M. S. Sadeh, "Seismic control of concrete shear wall using shape memory alloys," *Journal of Intelligent Material Systems and Structures*, vol. 23, no. 5, pp. 535–543, 2012.

[9] M. Ghassemieh, M. Rezapour, and V. Sadeghi, "Effectiveness of the shape memory alloy reinforcement in concrete coupled shear walls," *Journal of Intelligent Material Systems and Structures*, vol. 28, no. 5, pp. 640–652, 2017.

[10] M. Rezapour, M. Ghassemieh, M. Motavalli, and M. Shahverdi, "Numerical modeling of unreinforced masonry walls strengthened with Fe-based shape memory alloy strips," *Materials*, vol. 14, no. 11, p. 2961, 2021.

[11] S. Hesami and V. Sadeghi, "Numerical investigation of the shape memory alloy dowels in jointed concrete pavements," *International Journal of Pavement Research and Technology*, vol. 8, no. 4, pp. 251–258, 2015.

[12] B. Asgarian and S. Moradi, "Seismic response of steel braced frames with shape memory alloy braces," *Journal of Constructional Steel Research*, vol. 67, no. 1, pp. 65–74, 2011.

[13] M. Shariyat and M. Moradi, "Enhanced algorithm for nonlinear impact of rectangular composite plates with SMA wires, accurately tracing the instantaneous and local phase changes," *Composite Structures*, vol. 108, pp. 834–847, 2014.

[14] M. Shariyat, M. Moradi, and S. Samaee, "Enhanced model for nonlinear dynamic analysis of rectangular composite plates with embedded SMA wires, considering the instantaneous local phase changes," *Composite Structures*, vol. 109, pp. 106–118, 2014.

[15] R. Johnson, J. E. Padgett, M. Emmanuel Maragakis, R. DesRoches, and M. Saiid Saiidi, "Large scale testing of nitinol shape memory alloy devices for retrofitting of bridges," *Smart Materials and Structures*, vol. 17, no. 3, Article ID 035018, 2008.

[16] M. S. Saiidi, M. Sadrossadat-Zadeh, C. Ayoub, and A. Itani, "Pilot study of behavior of concrete beams reinforced with shape memory alloys," *Journal of Materials in Civil Engineering*, vol. 19, no. 6, pp. 454–461, 2007.

[17] M. S. Saiidi and H. Wang, "Exploratory study of seismic response of concrete columns with shape memory alloys reinforcement," *ACI Materials Journal*, vol. 103, no. 3, p. 436, 2006.

[18] S. M. R. Mortazavi, "Evaluating the effectiveness of a shape memory alloy on a connection equipped with slit damper," *Journal of Vibration Engineering & Technologies*, vol. 101, pp. 1–15, 2022.

[19] M. Shakiba and S. M. R. Mortazavi, "Analytical and numerical investigation of knee brace equipped with a shape memory alloy damper," *Shock and Vibration*, vol. 2022, Article ID 6797938, 15 pages, 2022.

[20] C. Fang, W. Wang, C. He, and Y. Chen, "Self-centring behaviour of steel and steel-concrete composite connections equipped with NiTi SMA bolts," *Engineering Structures*, vol. 150, pp. 390–408, 2017.

[21] W. Wang, C. Fang, and J. Liu, "Self-centering beam-to-column connections with combined superelastic SMA bolts and steel angles," *Journal of Structural Engineering*, vol. 143, no. 2, Article ID 04016175, 2017.

[22] S. K. Mishra, S. Gur, and S. Chakraborty, "An improved tuned mass damper (SMA-TMD) assisted by a shape memory alloy spring," *Smart Materials and Structures*, vol. 22, no. 9, Article ID 095016, 2013.

[23] O. E. Ozbulut, P. N. Roschke, P. Y. Lin, and C. H. Loh, "GA-based optimum design of a shape memory alloy device for seismic response mitigation," *Smart Materials and Structures*, vol. 19, no. 6, Article ID 065004, 2010.

[24] C. Qiu, T. Jiang, J. Liu, and X. Du, "Seismic performance of knee-braced frames equipped with NiTi BRBs," *Journal of Constructional Steel Research*, vol. 197, Article ID 107480, 2022.

[25] M. A. Conti, L. Mastrandrea, and V. Piluso, "Plastic design of seismic resistant knee braced frames," *Proceedings of STESSA*, vol. 12, pp. 14–17, 2006.

[26] H. Hsu, J. Juang, and C. Chou, "Experimental evaluation on the seismic performance of steel knee braced frame structures with energy dissipation mechanism," *Steel and Composite Structures*, vol. 11, no. 1, pp. 77–91, 2011.

[27] M. Mofid and P. Khosravi, "Non-linear analysis of disposable knee bracing," *Computers & Structures*, vol. 75, no. 1, pp. 65–72, 2000.

[28] M. Lotfollahi and M. Mofid, "On the design of new ductile knee bracing," *Journal of Constructional Steel Research*, vol. 62, no. 3, pp. 282–294, 2006.

[29] M. Mofid and M. Lotfollahi, "On the characteristics of new ductile knee bracing systems," *Journal of Constructional Steel Research*, vol. 62, no. 3, pp. 271–281, 2006.

[30] O. Z. Amer, E. M. Güneyisi, and A. Erdoğan, *Comparative Analysis of Bare and Knee Braced Frames under Earthquake Loading*, Çelik Yapılar Sempozyumu, Turkey, 2016.

[31] G. Aniello and G. Landolfo, "Seismic response of steel frames with knee braces," in *Proceedings of the 7th European Conference on Steel and Composite Structures*, Naples, Italy, September 2014.

[32] D. Lagoudas and M. Khan, *Shape Memory Alloys Modeling and Engineering Applications*, Springer, Berlin, Germany, 2008.

[33] D. Sumanth, K. L. Preetish, and S. M. Srinivasan, "A subspace thermodynamic model for shape memory alloy wire elements undergoing combined thermo-mechanical axial and torsional loads," *Smart Materials and Structures*, vol. 23, no. 8, Article ID 085027, 2014.

[34] T. Balendra, M. T. Sam, and C. Y. Liaw, "Diagonal brace with ductile knee anchor for aseismic steel frame," *Earthquake Engineering & Structural Dynamics*, vol. 19, no. 6, pp. 847–858, 1990.

[35] R. DesRoches, J. McCormick, and M. Delemont, "Cyclic properties of superelastic shape memory alloy wires and bars," *Journal of Structural Engineering*, vol. 130, no. 1, pp. 38–46, 2004.

[36] C.-X. Qiu and S. Zhu, "Performance-based seismic design of self-centering steel frames with SMA-based braces," *Engineering Structures*, vol. 130, pp. 67–82, 2017.

[37] M. Rezapour and M. Ghassemieh, "Macroscopic modelling of coupled concrete shear wall," *Engineering Structures*, vol. 169, pp. 37–54, 2018.

[38] S. M. R. Mortazavi and B. Zaeimdar, "Shear wall modeling with asymmetric openings by macro elements," in *Structures*, vol. 29, pp. 899–910, Elsevier, 2021.

[39] H. Krawinkler, "ATC-24 guidlines for cyclic seismic testing of components of steel structures," *Redwood City, Report prepared for the Applied Technology Council*, 1992.

[40] M. Ghassemieh, M. Rezapour, and A. Taghinia, "Predicting low cycle fatigue life through simulation of crack in cover plate welded beam to column connections," *Journal of Computational and Applied Mechanics*, vol. 48, no. 1, pp. 39–52, 2017.